JPET Fast Forward. Published on September 18, 2006 as DOI: 10.1124/jpet.106.108670

JPET #108670

ACETYLCHOLINE RELEASE AT NEUROMUSCULAR JUNCTIONS OF ADULT *TOTTERING* MICE IS CONTROLLED BY N– (Ca_v 2.2) AND R- (Ca_v 2.3), BUT NOT L-TYPE (Ca_v1.2) Ca^{2+}CHANNELS

Nicole E. Pardo, Ravindra K. Hajela and William D. Atchison
Department of Pharmacology and Toxicology
Michigan State University
East Lansing, MI 48824, USA

JPET #108670

Short Title: N– & R-type Ca^{2+} channels at NMJ in *tottering* mice

Address all correspondence to:

Dr. William D. Atchison, Ph.D.
Department of Pharmacology and Toxicology
Michigan State University
B-331 Life Sciences Bldg
East Lansing, MI 48824-1317, USA
phone: 517 353-4947
Fax: 517 432-1341
email: atchiso1@msu.edu

Document statistics:

Number of text pages:	47
Number of tables:	1
Number of figures:	9
Number of references:	49
Number of words in abstract:	249
Number of words in introduction:	782
Number of word in discussion:	1966

Abbreviations:

AChR: Acetylcholine receptor
DHP: Dihydropyridine
EDL: *Extensor digitoris longus*
FITC: Fluorescein isothiocyanate
m: Quantal content
O.C.T: Optimal Cutting Temperature
PBS: Phosphate-buffered saline
tg: *Tottering*
TRITC: Tetra methyl rhodamine isothiocyanate
TS: *Triangularis sterni*
ω-Aga IVA: ω-Agatoxin IVA
ω-CTx MVIIC: ω-conotoxin MVIIC
ω-CTx GVIA: ω-conotoxin GVIA

Abstract

The mutation in the α_{1A} subunit gene of the P/Q-type (Ca_v 2.1) Ca^{2+} channel present in *tottering* (*tg*) mice causes ataxia and motor seizures which resemble *absence* epilepsy in humans. P/Q-type Ca^{2+}channels are primarily involved in ACh release at mammalian neuromuscular junctions. Unmasking of L-type (Ca_v 1.1 - 1.2) Ca^{2+} channels occurs in cerebellar Purkinje cells of *tg* mice. However, whether L-type Ca^{2+} channels are also up-regulated at neuromuscular junctions of *tg* mice is unknown. We characterized thoroughly the pharmacological sensitivity of the Ca^{2+} channels which control ACh release at adult *tg* neuromuscular junctions. Block of N-and R-type (Ca_v2.2-2.3), but not L-type Ca^{2+} channels, significantly reduced quantal content of EPPs in *tg* preparations. Neither resting nor KCl-evoked MEPP frequency differed significantly between *tg* and wild type *(wt)*. Immunolabeling of Ca^{2+} channel subunits α_{1A}, α_{1B}, α_{1C}, and α_{1E} revealed an apparent increase of α_{1B}, and α_{1E} staining, at *tg* but not *wt* neuromuscular junctions. This presumably compensates for the deficit of P/Q-type Ca^{2+}channels, which localized presynaptically at *wt* neuromuscular junctions. No α_{1C} subunits juxtaposed with pre- or postsynaptic markers at either *wt* or *tg* neuromuscular junctions. Thus, in adult *tg* mice, immunocytochemical and electrophysiological data indicate that N- and R-type channels both assume control of ACh release at motor nerve terminals. Recruitment of alternate subtypes of Ca^{2+} channels to control transmitter release appears to

represent a commonly-occurring method of neuronal plasticity. However, it is unclear which conditions underlie recruitment of Ca_v2 as opposed to Ca_v1-type Ca^{2+} channels.

Introduction

Influx of Ca^{2+} through high voltage-activated Ca^{2+} channels triggers neurotransmitter release (Augustine and Charlton, 1986). Different Ca^{2+} channels are distinguished based on the genes which encode them and their pharmacological and biophysical characteristics.

Most of the subtype-specific attributes of Ca^{2+} channels are due to the α_1 subunit, which makes up the selective pore for Ca^{2+}, contains binding sites for various pharmacological agents, and possesses the gating regions of the channel (Zhang *et al.*, 1993). At least five α_1 subunits for neuronal Ca^{2+} channels are known. The α_{1A}, α_{1B}, and α_{1E} subunits represent the P/Q-type ($Ca_v2.1$), N-type ($Ca_v2.2$) and R-type ($Ca_v2.3$) Ca^{2+} channels, respectively. The α_{1C} or α_{1D} represent L-type channels ($Ca_v1.2$-1.3) (Tsien *et al.*, 1991). The anatomical location, time in development and age of the animal all affect the expression of specific Ca^{2+} channel subtypes; multiple phenotypes coexist in the same cell. This redundancy modulates critical functions by allowing the various channel subtypes to act in concert; however, distinct channel subtypes may also be differentially localized and spatially separated in the same cell.

Other factors also affect the expression and localization of Ca^{2+} channel subtypes. In mammals, ACh release from adult somatic motor nerve terminals is mediated predominantly by P/Q-type Ca^{2+} channels (Uchitel *et al.*, 1992) while in amphibians and birds, it is mediated by N-type Ca^{2+} channels (Robitaille *et al.*, 1990; De Luca *et al.*, 1991). P- and Q-type Ca^{2+} channels, originally described in cerebellar Purkinje and granule cells respectively (Llinás *et al.*,

1989; Randall and Tsien, 1995), are widely distributed and mediate neurotransmitter release at central and peripheral synapses. L-type Ca^{2+} channels can also contribute to secretory function. These participate in ACh release at neuromuscular junction in certain situations (Suguira and Ko, 1997 and Urbano *et al*., 2003). R- and N–type Ca^{2+} channels also substitute for P/Q-channels in controlling ACh release (Urbano *et al.*, 2003) at neuromuscular junction. The conditions which determine what subtypes of Ca^{2+} channel participate in secretory function are, as yet unclear, but have important implications for synaptic plasticity.

Several natural mutations of P/Q-type Ca^{2+} channels such as *tottering* (*tg*) have been identified in mice. They have been used to study inherited neurological disorders (Burgess and Noebels, 1999; Pietrobon, 2002). The *tg* mutation encodes a proline to leucine amino acid substitution in the S5-S4 linker region of repeat domain II of the α_{1A} subunit (Fletcher *et al*., 1996). This reduces whole cell current density and voltage-dependent inactivation during prolonged depolarization of Purkinje cells, without affecting single Ca^{2+} channel conductance (Wakamori *et al*., 1998). As a result, P/Q-type Ca^{2+} channel function is compromised, and neurotransmitter release at hippocampal and cerebellar synapses now depends predominately on N-type channels (Qian and Noebels, 2000; Zhou *et al.*, 2003). Stereotypic behavior is induced by the L-type agonist BayK 8644 in *tg* but not wild-type (*wt*) animals (Campbell and Hess, 1999). L-type channel α_{1C} subunit mRNA was also up-regulated in Purkinje cells (Campbell and Hess, 1999) and basal forebrain neurons (Etheredge *et al*., 2005) of *tg* mice, suggesting that

the L-type phenotype is newly expressed, or unmasked. In hippocampal slices taken from animals lacking P/Q-type Ca^{2+} channels (α_{1A} -/-), expression of functional non-P/Q- type channels is augmented. These changes included elevation of cerebellar Purkinje cell L- and N-type current density and reduction of cerebellar granule cell R- type current density (Jun *et al.*, 1999). Hence, expression of Ca^{2+} channels in a given cell type is not fixed, and up- or down-regulation of other Ca^{2+} channel subtypes can occur following mutation or ablation of P/Q- type Ca^{2+} channels.

The *tg* mutation, despite altering function of the primary subtype of Ca^{2+}channel normally involved in ACh release, does not cause neuromuscular dysfunction, aside from the obvious gait abnormality. Thus, some other Ca^{2+} channel subtype(s) assumes control of ACh release at *tg* neuromuscular junctions. Neuromuscular transmission in *tg* mice was investigated by Plomp *et al.*, (2000). Two alterations were observed: 1) run-down of release during high frequency nerve stimulation was increased; and 2) MEPP frequency was increased in a Ca^{2+}, Mg^{2+}, and K^{+} dependent manner. Recently, Kaja *et al.*, (2006) demonstrated a slight increase in R-type, but not N-type channel contribution in 6 wk old *tg* mice. However, Ca^{2+} channel expression is age-dependent, so this may not reflect the mature pattern of Ca^{2+} channel dependency of ACh release in these mice.

We sought to determine the pharmacological sensitivity of neuromuscular transmission of adult *tg* mice, specifically, whether loss of functional P/Q-type channels unmasks L-type or

another subtype of Ca^{2+} channels, and what Ca^{2+} channel subtypes sustain release in *tg* mice. Immunohistochemical and electrophysiological data were combined to provide an in-depth analysis of the pharmacological types of Ca^{2+} channels at adult *tg* motor nerve terminals.

Materials and Methods

Drugs and Chemicals.

Nimodipine, S-(-)-BayK 8644 and 4-(2-hydroxyethyl)-1-piperazineethanesulfonic acid (HEPES) were purchased from Sigma-Aldrich, Inc. (St. Louis, MO). μ-Conotoxin GIIIB and ω-conotoxin GVIA were purchased from Bachem, Inc. (Torrance, CA). ω-Agatoxin IVA and ω-conotoxin MVIIC were obtained from Alomone Labs (Jerusalem, Israel). SNX 482 was obtained from Peptides International (Louisville, KY). All chemicals obtained were of the highest purity available. Toxins were prepared as stock solutions in distilled water containing 0.01% bovine serum albumin (w/v), stored frozen at -20^{o}C, and were used within a 2-week period. Before incubation with any of the toxins, 0.01% bovine serum albumin was also added to the buffered saline solution to prevent nonspecific binding of toxin to the chamber, tubing, and glassware. Nimodipine was prepared as a 10 mM stock solution in 100% ethanol, and was kept in a dark bottle at 4^{o}C until use. The final working solution with nimodipine contained only 0.1% ethanol (v/v). All experiments using DHPs were done in a darkened room to avoid breakdown of the photolabile compound.

Antibodies against Ca^{2+} channel α_1 subunits (rabbit Anti - $Ca_v2.1$, P/Q-, Anti - $Ca_v2.2$, N–, Anti - $Ca_v1.2$, L-, and Anti - $Ca_v2.3$, R-type) were obtained from Alomone Labs. Fluorescein (FITC)-conjugated affinipure goat anti-rabbit IgG (Heavy + Light chains- H+L) was purchased from Jackson ImmunoResearch Laboratories, Inc. (West Grove, PA), Pacific Blue®

goat anti-mouse IgG (H+L) and tetramethylrhodamine α-bungarotoxin were obtained from Molecular Probes, Invitrogen Corp (Carlsbad, CA). Anti-mouse IgG1 monoclonal anti-syntaxin clone HPC-1 antibody was obtained from Sigma-Aldrich Inc.

Mice.

Breeding pairs of heterozygote C57BL/6J-*tg* mice were obtained from Jackson Laboratory (Bar Harbor, ME) and colonies maintained at Michigan State University Laboratory Animal Resources. Litters were genotyped at weaning, 3 weeks after birth (Plomp *et al.*, 2000). Although the genotype has been well described, because of differences between our results and those published previously (Plomp *et al*., 2000; Kaja *et al*., 2006), we verified the genotype of all mice used (results not shown). Homozygote (*tg/tg*) mice were also identified by their characteristic phenotype consisting of a mild ataxia and occasional attacks of dyskinesia. For all the experiments we used male mice between 3 to 9 months of age. All experiments were performed in accordance with local university (Michigan State University Laboratory Animal Resources) and national (NIH) guidelines and were approved by the University Animal Use and Care Committee.

Electrophysiology.

Animals were sacrificed by decapitation following anesthesia with 80% CO_2 and 20% O_2. The diaphragm muscle with its attached phrenic nerves was then removed and pinned out at resting tension in a Sylgard-coated chamber. For control recordings, the tissue was perfused continuously at a rate of 1-5 ml/min with oxygenated (100% O_2) physiological saline solution containing 137.5 mM NaCl, 5.0 mM KCl, 1 mM $MgCl_2$, 11 mM D-glucose and, 4 mM HEPES and remained at room temperature. pH was adjusted to 7.4 at room temperature (23-25^{o}C) using NaOH. Muscle action potentials were inhibited by pretreating the tissue with μ-conotoxin GIII B (2.5-4 μM) for 15 min. This toxin preferentially blocks muscle Na^+ channels (Cruz *et al.*, 1985; Hong and Chang, 1989), and thus suppresses muscle contractility. This technique allowed recording of EPPs from intact myofibers without the complicating effects of depressing ACh release or blocking post-junctional ACh receptors as would occur in high [Mg^{2+}] low [Ca^{2+}] or *d*-tubocurarine-treated preparations respectively. Given that during the electrophysiological recordings the preparations were continuously perfused with physiological saline at a rate of 1-5 ml/min, they were re-treated with μ-conotoxin GIII B (2.5-4 μM) for 15 min, after ~ 60-90 min, to maintain contractile block.

Involvement of L-type channels in ACh release was determined by testing their sensitivity to the L-type DHP antagonist, nimodipine and agonist BayK 8644 (Atchison, 1989). Paired comparisons were made for each preparation between the drug-free treatment (control), BayK 8644 and following application of BayK 8644 in the presence of nimodipine. Values are

expressed as the percentage of quantal content (*m*) from drug-treated preparations to that of preparation before addition of the drug (control). Similarly, sensitivity to ω- conotoxin GVIA (ω-CTx GVIA), SNX 482, ω-agatoxin IVA (ω-Aga IVA), and ω-conotoxin MVIIC (ω-CTx MVIIC) was used to test for the contribution of N-, R-, P-, and Q-type Ca^{2+} channels respectively, to ACh release at *tg* motor nerve terminals. Cd^{2+} was used to block all Ca^{2+} channels nonspecifically. The P/Q-, N- and R- type antagonists are all essentially irreversible, so only one toxin or drug was applied to any preparation. Two protocols were used to apply toxins. Because of the high concentrations used for the ω-CTx MVIIC (5 μM) study and the initial concentration-response relationship for ω-Aga IVA (up to 300 nM), for these studies the hemidiaphragm was preincubated in 5 ml of solution containing the corresponding toxin for 1 h before commencing electrophysiological recordings. The solution was constantly aerated with 100% O_2. For all other experiments (final ω-Aga IVA responses, ω-CTx GVIA, SNX 482, nimodipine, BayK 8644, and Cd^{2+}) the hemidiaphragm was superfused with the constantly oxygenated (100% O_2) solution in which the specific toxin or compound was diluted. ω-Aga IVA, ω-CTx GVIA and SNX 482 were used at 100 nM, 3 μM and 1 μM respectively, and diluted in 10 ml of physiological saline solution. Nimodipine, BayK 8644, and Cd^{2+} were used in concentrations of 10, 1 and 10 μM respectively, and diluted in 20 ml of physiological saline solution. These concentrations were chosen based on literature determining their effectiveness

at murine neuromuscular junctions (cf: Atchison, 1989; Xu *et al.*, 1998; Santafe *et al.*, 2000; Urbano *et al.*, 2001, 2003; Flink and Atchison, 2002; Kaja *et al.*, 2006).

MEPPs and EPPs were recorded using intracellular glass microelectrodes (1.0 mm o.d.; WPI, Sarasota, FL, USA) having a resistance of 5-15 MΩ when filled with 3 M KCl and localized at the end-plate. The phrenic nerve was stimulated at 0.5 Hz with constant current, using a duration of 50 μsec, by means of a suction electrode attached to a stimulus isolation unit (Grass SIU; Grass Instruments, Quincy, MA) and stimulator (Grass S48). Signals were amplified using a WPI 721 amplifier, digitalized using a PC-type computer and Axoscope 9.0 (Axon Instruments, Foster City, CA) software and analyzed using MiniAnalysis 6.0 software (Synaptosoft, Decatur, GA).

Control recordings were made from neuromuscular junction preparations isolated from *tg*/*tg*, C57BL/6J-*tg* and *wt* mice without any treatment, and following incubation with the individual chemical or toxin for 1 h. For each preparation, recordings from 5-10 end-plates were sampled and averaged to determine the mean amplitude of the EPPs and MEPPs before and after addition of any pharmacological treatment, yielding an *n* value of 1. Each end-plate was sampled for over 5 min, and the last end-plate recorded from, before any treatment, was the first end-plate recorded from after treatment. Amplitudes of MEPPs and EPPs were normalized to a membrane potential of -75 mV using the formula: Vc = [Vo * (-75)]/ E, where Vc is the corrected EPP/MEPP amplitude, Vo is the observed EPP/MEPP amplitude and E is the resting

membrane potential. Recordings were rejected if the 10-90% rise time was greater than 1.5 ms or if the membrane potential was more depolarized than -55 mV. The normalized EPPs were corrected for non-linear summation (McLachlan and Martin, 1981) using the formula $V_{corr} = V[(1-0.8V)\ E^{-1}]^{-1}$, where V is the uncorrected EPP amplitude, E is the resting membrane potential, and V_{corr} is the corrected EPP amplitude. Quantal content (*m*) was calculated using the ratio of the mean amplitude of the corrected EPPs and MEPPs. The effects of nerve terminal depolarization, induced by raising the $[K^+]_e$ from 2.5 to 5, 10 and 20 mM, on MEPP frequency were also measured. After a brief period to permit the bath fluid to reach the new $[K^+]_e$ (usually 2 min), at least 5 min of MEPPs were recorded at each $[K^+]_e$. When $[KCl]_e$ was raised, equimolar reductions in $[NaCl]_e$ were made.

Separate preparations were used for each unique experiment conducted. For pharmacological studies, each animal served as its own control. Experiments were replicated in at least 5 animals. The number of animals used in any given experiment is indicated in the respective figure legend or table. Statistical significance between the various treatment groups was analyzed using a one-way analysis of variance (Prism Statistical Software, Graphpad Software, El Camino Real, CA). *Post-hoc* differences among sample means were analyzed using Tukey's test. For all experiments, statistical significance was set at $p < 0.05$. Pre-drug values for all the animals of a given genotype (*wt,* C57BL/6 J-*tg, tg/tg*) were pooled, as the between-animal variance was homogeneous for that group (Graphpad Statistical Software, Graphpad Inc.).

Immunohistochemistry.

Localization of the different Ca^{2+} channel α_1 subunits at *tg* and *wt* mouse motor nerve terminals was compared using fluorescence immunohistochemistry in the *extensor digitorum longus* (EDL) and *triangularis sterni* (TS) muscles from animals whose diaphragm was used for pharmacological studies. The EDL is a homogeneous fast twitch type muscle, and thus concerns associated with myofiber-type dependent differences in structure or function of the neuromuscular junctions were minimized (Gertler and Robbins, 1978; Prakash *et al.*, 1996). The thinness of the TS muscle allowed us to label neuromuscular junction structures without using cryo-sectioning techniques that involved prolonged exposure of the preparation to chemicals such as sucrose, yet permitted high quality images to be obtained. The fiber type of TS muscle is not known. Qualitatively, results obtained from EDL and TS preparation were consistent, showing the same characteristics of distribution among the different α_1 subunits studied at neuromuscular junctions. No attempt was made to quantify potential differences in staining between the two muscle types. Both muscles were pinned out and lightly fixed for 30 min at room temperature in 4% (w/v) paraformaldehyde in 0.1 M phosphate-buffered saline (PBS; composition (in mM): NaCl 137, KCl 2.7, NaH_2PO_4 1.4, Na_2HPO_4 4.3, pH 7.4). The preparation was then washed in PBS for 1 min and treated with 0.1% (w/v) Triton X-100 in PBS for 30 min. EDL tissue was subsequently washed for 15 min and cryoprotected in 20% and 30% (w/v)

sucrose each for 24 h. After 48 h, blocks of tissue were embedded in O.C.T. (Optimal Cutting Temperature) compound (Tissue-Tek, Tokyo, Japan) in a plastic mold on dry ice and stored at -80^{o} C until used. Longitudinal and cross sections (30 μm thick) were cut on a cryostat (Model 5040, Bright Microtome, Bright Instrument Company Ltd., Huntingdon, Cambridge, England) and mounted onto gelatin-coated slides. Because the TS muscle is extremely thin, no cryosectioning was needed. Preparations were double- or triple-labeled using α-bungarotoxin as a marker for the postsynaptic ACh receptors at the motor end-plate, commercially available monoclonal anti-syntaxin antibody, labeled subsequently with Pacific Blue® tagged secondary antibody as a presynaptic marker and antibodies to the various α_1 subunits of the Ca^{2+} channels, labeled subsequently with fluorescein isothiocyanate (FITC) tagged secondary antibody. Preliminary experiments with *wt* preparations demonstrated the expected juxtaposition of presynaptic syntaxin with postsynaptic α-bungarotoxin (Fig. 5). Thus these experiments were replicated in only a limited number of preparations because the confocal microscope used for fluorescence quantitation has only two lasers, and hence could not support simultaneous collection of data at 3 wavelengths. The preparations were washed in PBS for 15 min and then incubated at 4^{o}C overnight (~15 h) with the subunit-specific primary antibody and antisyntaxin antibody. After washing for 1 h with PBS, sections were incubated for 1 h in fluorescently-labeled secondary antibodies, together with rhodamine labeled α-bungarotoxin. After several washes, the preparation was mounted with anti-fading fluorescent mounting medium

(Vectashield® Hard Set, Vector Laboratories, Burlingame, CA). The different color fluorescent signals were collected and integrated using a Leica TCS SL laser scanning confocal microscope (Leica Microsystems, Exton, PA) to determine the spatial localization and distribution of the α_1 subunits relative to the motor end-plate. This microscope allows simultaneous scanning of FITC and TRITC, which were excited at 510-nm and 580-nm, respectively, using an argon/HeNe-G laser. All pictures of the immunofluorescent signals were taken with the same confocal configuration settings (laser intensity, time exposure resolution and magnification) for each antibody tested. Integrated signals for the different fluorophores were used to generate composite images for determining spatial localization and distribution of fluorescence. In addition, to determine the spatial localization and distribution of the α_1 subunits and syntaxin relative to the motor end-plate, some preparations were also viewed on a Nikon Elipse 2000-U Diaphot-TMD microscope (Nikon Inc., Melville, NY) with a Hamamatsu Orca 285 CCD camera (Bridgewater, NJ) and images acquired using MetaImaging software suite, (Universal Imaging Imaging Corp., Downington, PA). This system allows simultaneous composite viewing of sequentially acquired images of FITC, TRITC and Pacific Blue labeled samples. For each TS preparation, three to five surface nerve terminals were selected for quantitation of relative fluorescence levels. Since all pictures were taken using the same confocal configuration settings, we used ImageJ software (NIH) to calculate and average the fluorescence levels from total pixels corresponding to the green dye in each picture. Averages of the mean values of

fluorescence obtained from all the individual nerve terminals sampled were calculated for each specific α_1 subunit studied. Averaged values of fluorescence were compared between the *tg* and the *wt* preparations using the values obtained from the *wt* preparation as control values. Subsequently, the percentage of juxtaposition of the green and the red dye was calculated by dividing the surface of each picture taken into an area of 5 by 5 squares for a total of 25 inner squares. Each inner square in which the green and the red dyes were juxtaposed was taken as 4% of juxtaposition.

Results

Table 1 compares the amplitudes of EPPs and MEPPs, MEPP frequency and quantal content (*m*) for *tg/tg* and *wt* mice. When supramaximal electrical stimuli were delivered to the phrenic nerve at 0.5 Hz, the mean amplitude of EPPs and *m* in *tg/tg* preparations did not differ significantly ($p > 0.05$) from the value obtained in the *wt* preparations. Similarly, the mean amplitude and frequency of spontaneously-occurring MEPPs did not differ between *wt* and *tg/tg* preparations. Thus, as suggested by their gross phenotype, neuromuscular transmission in *tg/tg* mice is not significantly compromised compared to that of *wt*.

An identical set of experiments were performed in heterozygote C57BL/6J-*tg* preparations, and the results did not differ significantly from those obtained from *wt* preparations (data not shown).

The P/Q-type Ca^{2+} channel antagonist ω-Aga IVA reduced *m* of EPPs in *wt*, C57BL/6 J-*tg* and *tg/tg* preparations, however this reduction was statistically significant in only the C57BL/6 J-*tg* and *wt* preparations ($p < 0.05$) (Fig. 1A). ω-Aga IVA (100 nM) reduced *m* in C57BL/6 J-*tg* by 60% (Fig. 1A), compared to the ~80% reduction in the *wt* preparation, however the difference between these two groups was not significant ($p > 0.05$). Thus, the heterozygotes (C57BL/6 J-*tg*) neuromuscular junctions apparently behave as a normal *wt*. Perhaps the expression of the normal α_{1A} subunit protein of the P/Q-type Ca^{2+} channels is not sufficiently reduced in the C57BL/6 J-*tg* (heterozygotes) to cause alteration in the normal

function of the P/Q-type channels. Consequently, there may be no need for compensation of function through other channel phenotypes.

The pharmacological sensitivity of the heterozygotes to other Ca^{2+} channel antagonists was also examined. These results are shown for all drugs tested in Figure 1A. For none of these drugs, did the C57BL/6J-*tg* heterozygote response differ significantly from those of *wt* ($p > 0.05$). Thus for ease of comparison, the following focus is on the comparison of the *tg/tg* (*tg*) and *wt* groups.

L-type Ca^{2+} channels do not contribute to release of ACh at *tg* neuromuscular junction.

Nimodipine (an L-type antagonist) and BayK 8644 (an L-type agonist) were used to examine whether L-type Ca^{2+} channels contribute to release of ACh at *tg* motor nerve terminals. As shown in Figure 1B, 10 μM nimodipine reduced *m* by 16.3 ± 3.8 % of nimidopine-free treatment value (control) in *wt* preparations and by only 4.7 ± 2.9 % in *tg* preparations. Neither of these effects was statistically significant ($p > 0.05$). Subsequently the preparation was washed with a nimodipine-free solution for 5 min or until EPP amplitude returned to baseline. Subsequent addition of a solution containing BayK 8644 caused a 12.9 ± 3.8 % increase in *m* at *wt* preparations but essentially had no effect, at *tg* preparations. This slight increase in *m* induced by BayK 8644 in the *wt* could be prevented by pretreatment with nimodipine (Fig. 1B).

JPET Fast Forward. Published on September 18, 2006 as DOI: 10.1124/jpet.106.108670
This article has not been copyedited and formatted. The final version may differ from this version.

Neuromuscular transmission in *tg* mice is poorly susceptible to the P/Q-type antagonists ω-Aga IVA and ω-CTx MVIIC.

The effects of P/Q-type antagonist ω-Aga IVA (100 nM) on EPP amplitude of *tg* and *wt* genotypes are shown for representative examples (Panels B-C) in Figure 3. Comparing the effects of the two toxins on *m* revealed that ω-Aga IVA (100 nM) decreased *m* by ~22% in *tg* and ~ 82.4% in *wt* preparations (Fig. 3A). Higher concentrations of ω-Aga IVA (300 nM) had no additional effect in *m* in *tg* preparations (Fig. 2). Similarly, ω-CTx MVIIC reduced *m* by 92.4% in *wt* and 41.3% at *tg* neuromuscular junctions. Thus, while the two toxins affected each of the two genotypes, 1) a greater effect was seen with the less specific ω-CTx MVIIC than with ω-Aga IVA, and 2) the effect of each toxin was greater in the *wt* than the *tg* neuromuscular junctions.

N- and R-type Ca^{2+} channels contribute to the majority of nerve-evoked ACh release at *tg* neuromuscular junctions.

The contribution of N- and R-type Ca^{2+} channels to ACh release from *tg* mice was tested using ω-CTx GVIA (3 μM) and SNX 482 (1 μM) respectively. Figure 4 (Panels A-D) shows representative tracings of the comparative effects of ω-CTx GVIA and SNX 482 applied alone, or in combination, on EPP amplitude in *wt* and *tg* mice. Neither toxin alone nor in combination was effective in *wt* preparations. Conversely, both ω-CTx GVIA and SNX 482 significantly

reduced EPP amplitude in the *tg* preparations ($p < 0.05$). The combination of ω-CTx GVIA and SNX 482 caused a further and significant reduction in EPP amplitude of *tg* mice. However, even the combined presence of the two toxins did not completely abolish EPPs in *tg* mice. While each toxin caused significant reduction in *m* as compared to pretreatment control for *tg* preparations, comparing across genotypes, the effects in *tg* were only statistically significant from *wt* for SNX 482 and the combined treatment of SNX 482 and ω-CTx GVIA (Fig. 4B). Thus Ca^{2+} channels sensitive to SNX 482 and ω-CTx GVIA play a dominant role in neurotransmitter release at the *tg* motor nerve terminals.

For comparative purposes Cd^{2+}(10 μM) was applied to some preparations to block all Ca^{2+} channels nonspecifically. This concentration of Cd^{2+} completely blocked ACh release in *tg* as well as *wt* neuromuscular junctions (data not shown). Thus even though ACh release was not completely blocked by N– or R-type Ca^{2+} channel antagonists in the *tg* neuromuscular junction, it was totally sensitive to $Cd^{2+}$and in the same concentration range as was *wt*.

K^+ induced ACh release does not differ between *tg* and *wt* mice.

Voltage-dependent inactivation of Purkinje cell P/Q-type channels in *tg* mice is reduced (Wakamori *et al*., 1998) during prolonged depolarization. As such, we tested whether differences could be detected between *tg* and *wt* in MEPP frequency during prolonged KCl induced depolarization. Asynchronous evoked release of ACh was measured at different $[K^+]_e$

as increased MEPP frequency. Increasing $[K^+]_e$ incrementally from 2.5 to 20 mM increased MEPP frequency to equivalent levels in both preparations. ($p > 0.05$, results not shown)

Differential localization of voltage-dependent- Ca^{2+} channel α_1 subunits at *tg* and *wt* motor nerve terminals.

The distribution of α_{1A}, α_{1B}, α_{1C} and α_{1E} Ca^{2+} channel subunits at *tg* neuromuscular junction, was examined using fluorescence immunohistochemistry in sections of mouse *EDL* and *TS* muscles. The relative localization of these subunits with respect to the motor end-plates was assessed by comparing staining for subunit-specific antibodies to Ca^{2+} channels with that of fluorescent α-bungarotoxin to label postsynaptic ACh receptors, and anti-syntaxin antibody to label the presynaptic membrane.

As shown for the representative images in Figure 5, for both *wt* and *tg* mice intense staining occurred with antibody against syntaxin (blue) and α-bungarotoxin (red). The two stains were highly juxtaposed. Though not evident at the level of resolution of these images (results not shown), anti-syntaxin staining frequently exhibited a punctate pattern, as described by Santafe *et al*. (2005).

Figure 6 demonstrates the punctate distribution of α_{1A} subunit staining seen in *wt* preparations. As depicted in the representative images, the α_{1A} subunit staining was highly juxtaposed with that of the α-bungarotoxin labeled end-plate. The panels on the right of each

image depict quantitation of the extent of staining, and it's superimposition. The distribution and juxtaposition of the two stains is consistent with results described by Day *et al*. (1997). However this pattern of distribution was not observed in the *tg* preparations. There was little staining of *tg* preparations with anti-α_{1A} antibody, and what staining occurred did not juxtapose with the clearly demarcated end-plate.

The pattern of immunofluorescent staining for α_{1B}, α_{1C} and α_{1E} was quite different from that of α_{1A}. In the *wt* preparations, α_{1B} and α_{1E} labeling appeared to be randomly distributed, if it occurred, and it definitely did not juxtapose with α-bungarotoxin labeling (results not shown). However in the *tg* group, α_{1B} and α_{1E} subunit labeling demonstrated expression of both subunits, with some of the staining distributed along the vicinity of the end-plates, and some degree of juxtaposition with the α-bungarotoxin label (Fig. 7). Immunofluorescence distribution of the α_{1C} subunit appeared to run along the muscle fiber in the *wt* preparations (result not shown). No α_{1C} staining was observed at any of the *tg* motor nerve terminals.

The relative amount of fluorescence for each subunit is compared quantitatively across all preparations for the two genotypes in Figure 8. There was a significant increase in the amount of fluorescence corresponding to α_{1B} (124 ± 6.4 %) and especially to the α_{1E} (2283 ± 10.4 %) subunits in *tg* preparations compared to *wt*. As expected, the level of staining of α_{1A} was significantly higher in *wt* than *tg* preparations. There was no difference quantitatively between the two genotypes in staining for α_{1C}, which was negligible in each case.

JPET Fast Forward. Published on September 18, 2006 as DOI: 10.1124/jpet.106.108670
This article has not been copyedited and formatted. The final version may differ from this version.

As a further investigation of the descriptive results obtained in the initial immunohistochemical studies, we quantitated the extent of juxtaposition of α_1 subunit immunofluorescence with that of α-bungarotoxin (Fig. 9). Confocal microscopic imaging demonstrated that 69% of the α_{1A} labeling was juxtaposed with α-bungarotoxin labeling in the *wt* preparation, but only ~ 19% in the *tg* preparation. Surprisingly, the percentages of juxtaposition for α_{1B} and α_{1E} subunit labeling in *tg* preparations were only 12.5 and 15% respectively; there was no juxtaposition of either of these subunits with α-bungarotoxin in the *wt* preparations (Fig. 9). As described above, α_{1C} subunit appeared to run along the muscle fiber in the *wt* preparations with a percentage of juxtaposition of 16.66% within the end-plates. No α_{1C} subunit staining was juxtaposed with α-bungarotoxin in the *tg* group.

JPET Fast Forward. Published on September 18, 2006 as DOI: 10.1124/jpet.106.108670
This article has not been copyedited and formatted. The final version may differ from this version.

Discussion

P/Q-type channels are the normal primary regulators of nerve-evoked ACh release at mammalian neuromuscular junctions (Uchitel *et al*., 1992; Sugiura *et al*., 1995), so one might predict that α_{1A} subunit mutations in these channels would disrupt murine junctional transmission. However, *tg* mice exhibit no obvious neuromuscular impairment, hence P/Q-type channel function is somehow compensated.

This study characterized throughly, plasticity of ACh release at motor end-plates in these animals. Effects of the *tg* mutation on neuromuscular transmission have not been extensively studied. Kaja *et al*., (2006) suggested a possible compensation of non-$Ca_v2.1$ channels to evoked ACh release at 6 wk old *tg* motor nerve terminals. ω-Aga IVA reduced release by ~75% in *tg* preparations, as opposed to ~95% in *wt*. Additionally, ~15% sensitivity to SNX 482 and no sensitivity to ω-CTx GVIA occurred in *tg* preparations. Our study corroborates some of these findings, but differs in several ways. Moreover it extends them considerably.

Our results are consistent with the following conclusions: 1) P/Q-type channels contribute poorly to ACh release at adult *tg* neuromuscular junction, albeit heterozygote neuromuscular transmission is essentially similar to *wt*. 2) L-type channels do not contribute to ACh release in *tg* mice. 3) N- and R-type channels assume ACh release control in adult *tg* motor nerve terminals, however, some release remains insensitive to all toxins but equally

sensitive to Cd^{2+}. 4) At low rate (0.5 Hz) of stimulation, *m* does not differ between *wt* and *tg*. 5) No apparent differences occur in spontaneous release between adult *tg* and *wt* preparations.

The differential effect of ω-Aga IVA on *wt* and *tg* heterozygotes was not significant, although it displayed an interesting trend: ω-Aga IVA-sensitive channels contribute ~ 82 % to ACh release at *wt*, ~ 60 % at C57BL/6 J-*tg*, but only ~22% at *tg* neuromuscular junctions. Thus, fundamentally, the heterozygote neuromuscular junction behaves similar to *wt*. Adult *tg* mice Ca^{2+} channels showed higher sensitivity to the less specific blocker ω-CTx MVIIC than to ω-Aga IVA. Possible explanations for this result include: 1) the Q-type splice variant is more preponderant functionally than is the P-type in *tg* animals. 2) The ω-CTx MVIIC binding site is more accessible in the *tg* mice than is the ω-Aga IVA site. 3) The selectivity of ω-CTx MVIIC, especially at concentrations as high as 5 μM, is markedly reduced and it also blocks N-type channels (McDonough *et al*., 2002). Greater contribution of N-type channels at *tg* motor axon terminals could be reflected in the greater reduction of *m* by ω-CTx MVIIC. This finding is consistent with the subsequent sensitivity of *tg* neuromuscular transmission to ω-CTx GVIA. In either case, function of P/Q-type channels is markedly reduced in adult *tg* mice. In this regard, our results differ significantly from those of Kaja *et al*. (2006), who found a higher percentage of sensitivity to ω-Aga IVA in 6 wk old *tg* mice. Sensitivity to ω-CTx MVIIC was not reported. As described below, difference in age of the animals used may contribute to the differences in sensitivity between these studies.

A major question we sought to answer was whether L-type channel function was evident at *tg* neuromuscular junctions. L-type channels are up-regulated in cerebellum (Campbell and Hess, 1999) and basal forebrain (Etheredge *et al.*, 2005) of *tg* mice, however we found no contribution of L-type channels to ACh release at adult *tg* neuromuscular junctions. Up-regulation of L-type channels is a well-reported form of plasticity at murine neuromuscular junction. It occurs in adult mice treated chronically with Lambert Eaton Myasthenic Syndrome plasma (Smith *et al.*,1995, Xu *et al.*, 1998, Flink and Atchison 2002), reinnervating motor endplates following acute nerve damage (Katz *et al.*, 1996) or botulinum toxin-poisoned nerve terminals (Santafe *et al.,* 2000). L-type channels are also involved in ACh release in neonatal rats (Sugiura and Ko, 1997). While it is possible that L-type channel function at *tg* neuromuscular junctions is masked by the presence of other channel types such as Ca^{2+}-dependent K^+ channels (Flink and Atchison, 2003), immunolabeling does not reveal α_{1C} subunit staining at *tg* neuromuscular junctions. Thus L-type channel compensation is not generalized either to mutation, or ablation of P/Q-type channels.

ACh release in *tg* motor nerve terminals is sensitive to the N- and R-type channel antagonists ω-CTx GVIA and SNX 482 respectively. The immunolabeling demonstrates increased fluorescence for α_{1B}, but especially for α_{1E} in *tg* mice. Pharmacological studies also demonstrated a greater contribution of R- as opposed to of N-type channels to release. Hence, both types of data suggest a relocation-recruitment, or up-regulation of α_{1B} and α_{1E} subunits at *tg*

neuromuscular junctions. Presumably, this occurs to compensate for the loss of function of α_{1A} subunits. These channel subtypes apparently act synergistically in *tg* mice. This response is identical to that seen at neonatal mouse neuromuscular junctions of P/Q-type nullzygotes (Urbano *et al.*, 2003). In CNS nerve terminals in *tg* mice, N-type channels apparently are solely responsible for (Qian and Noebels, 2000) or predominate in controlling glutamate release (Leenders *et al.*, 2002; Zhou *et al.*, 2003). Neither of these studies tested responsiveness to SNX 482, and in neither case did ω-CTx GVIA completely abolish release, so it is possible that an R-type component contributed to glutamate release in their experiments. We observed no significant changes at *wt* neuromuscular junction with either of these pharmacological treatments, and heterozygotes did not express sensitivity to ω-CTx GVIA (SNX 482 was not tested). Consequently, N- and R-type channels primarily mediate ACh release at *tg* neuromuscular junctions. Why multiple subtypes of Ca^{2+} channels are necessary to replace a process which is normally almost exclusively dependent on a single subtype of Ca^{2+} channel is unclear.

The finding of contributions of both N- and R-type channels to ACh release differs from those of Kaja *et al*., (2006). They saw no effect of ω-CTx GVIA and only a modest reduction of *m* (15%) with SNX 482. The percent reduction of ACh release caused by ω-CTx GVIA in our study was virtually identical to that in cerebellar synaptosomes (Zhou *et al.*, 2003). The Kaja *et al.* (2006) study did not include immunohistochemical data, so it's unknown whether N-type

channels were present at *tg* motor nerve endings, but didn't contribute to ACh release. Differences between our two studies are most likely due to age-related factors. Several studies have demonstrated developmental changes in Ca^{2+} channel expression (Gray *et al*., 1992; Rosato Siri and Uchitel 1999). Full expression of α_{1B} and α_{1E} subunits may not occur until later than 6 weeks postnatal in *tg* mice. Thus at the comparatively young age of mice in which Kaja *et al*. (2006) examined neuromuscular function, there may have been a greater dependence on P/Q-type (hence the larger percent sensitivity of their animals to ω-Aga IVA), and a lesser contribution of N- or R-type channels (slight sensitivity to SNX 482 and no sensitivity to ω-CTx GVIA) than in 3-9 month old animals we used.

Although our results support up-regulation of R-type Ca^{2+} channels as a compensatory mechanism for the functional loss of P/Q-type channels at *tg* neuromuscular junctions, reports suggest that SNX 482 may not only block R-type but also P/Q- (Arroyo *et al.,* 2003) and N-type channels (Neelands *et al*., 2000). However, our immunohistochemical studies correlate with the pharmacological studies in that α_{1B} and α_{1E} staining is clearly evident at *tg* neuromuscular junctions, lending credence to the notion that R-type channels are present at *tg* terminals, and play an important role in ACh release. Similar findings are described (Pagani *et al*., 2004) at α_{1A} knockout neuromuscular junctions. Neither our pharmacological, nor immunohistochemical results suggested presence of R-type channels at *wt* neuromuscular junction.

Considerable phenotypic difference exists between the α_{1A} knockout and *tg* mouse, both of which have impaired P/Q-type channel function, and show compensatory increases in N- and R-type channels. In α_{1A} knockout mice, deletion of P/Q-type channels is lethal (Fletcher *et al.*, 2001), despite compensatory plasticity changes in Ca^{2+} channel phenotype (Jun *et al.*, 1999). Conversely, in *tg* mice, although the single amino acid substitution results in largely dysfunctional P/Q-type channels, some sensitivity to ω-Aga IVA remains even into adulthood. Nonetheless, other non P/Q-type Ca^{2+} channels are recruited to control ACh release and this release is sufficient to support normal neuromuscular function to adulthood. Perhaps the presence of a small fraction of P/Q-type channels in the *tg* mice suffices to permit function until sufficient recruitment of non-P/Q-type channels occurs. If this is the case, the fact that in *tg* mice α_{1A} protein is still expressed, albeit impaired functionally, may allow normal organization of the release apparatus and hence survival.

Despite the importance of SNX 482-sensitive ACh release to *tg* neuromuscular transmission, an aspect of the immunohistochemical data is puzzling. Although staining for α_{1E} was greater than that of α_{1B} in *tg* mice (Fig. 8), the percent juxtaposition of α_{1E} staining with α-bungarotoxin was low, in fact, no higher than that of α_{1A} or α_{1B} (Fig. 9). This implies that the R-type channels may not be closely localized to active zones. Urbano *et al.* (2003) suggest that there is a "preferred order" of insertion of high-voltage-activated Ca^{2+} channels into nerve terminal membrane in the active zones. R-type channels are suggested to be "preferred" over N-

type. Certainly our data indicate more control by R- than N-type channels of release in *tg* mice, but one would have expected a greater level of juxtaposition of the α_{1E} staining with the α-bungarotoxin than was observed. More extensive analyses of this will be needed to resolve this conundrum.

Earlier reports (Plomp *et al.*, 2000; Kaja *et al.*, 2006) indicated that resting MEPP frequency and response to depolarization with 10 mM KCl was increased in *tg* mice. However, we found *no* increase in resting MEPP frequency in either *tg* or C57BL6/*tg* mice, and the response to sustained depolarizations at [KCl] up to 20mM was equivalent in *tg* and *wt* mice. The basis for this difference in result may be methodological. While no details of the MEPP recordings were provided in Plomp *et al.* (2000), Kaja *et al*. report measuring at least 30 MEPPs at each neuromuscular junctions. At the reported frequencies in their paper (2.04 MEPPs/sec in *tg*, 0.96 MEPPs/sec in *wt*), this implies recordings of as little as 15-30 sec. We sampled over a much longer interval. At a frequency of 1Hz, for 5 min (our minimum sampling duration) we would sample ~300 MEPPs. Short time intervals could easily magnify apparent differences in MEPP frequency which would "average out" over longer intervals. This is especially true if "clusters" of MEPPs occurred (Fatt and Katz, 1952; Kriebel and Stolper, 1975; Vautrin and Kriebel, 1991) for whatever reason during a brief recording episode. Alternatively, perhaps younger mice exhibit a greater difference in MEPP frequency between the two genotypes. This would need to be examined more rigorously, however, to substantiate.

In conclusion, the type of channel which can control ACh release at mammalian neuromuscular junction is not fixed. R- and N-type Ca^{2+} channels contribute to ACh release at mammalian neuromuscular junctions under specific conditions such as following P/Q-type channel ablation in α_{1A} knockout animals (Jun *et al.*, 1999; Urbano *et al.*, 2003) or P/Q-type channel mutation. Therefore, recruitment of alternate subtypes of Ca^{2+} channels to overcome deficiency in the normal complement appears to represent a commonly-occurring method of neuronal plasticity. However, the identity of the compensatory type of Ca^{2+} channel(s) is not constant. Furthermore, even in the same genotype, plasticity varies from CNS to peripheral synapses. In each case, the apparent goal is to preserve synaptic function. However, different α_1 subunits have distinct biophysical as well as pharmacological properties, so substitution of one phenotype of Ca^{2+} channel with another is unlikely to be "seamless". The "rules" by which this up-regulation occurs, are not yet clear, but could play an important role in determining compensation at synapses in which Ca^{2+} channel function is altered.

Acknowledgements

The excellent word processing assistance of Erin E. Koglin and Tara S. Oeschger is especially appreciated.

References

Arroyo G, Aldea M, Fuentealba J, Albillos A, and Garcia AG (2003) SNX482 selectively blocks P/Q Ca^{2+} channels and delays the inactivation of Na^{+} channels of chromaffin cells. *Eur J Pharmacol* **475:**11-18.

Atchison WD (1989) Dihydropyridine-sensitive and -insensitive components of acetylcholine release from rat motor nerve terminals. *J Pharmacol Exp Ther* **251:**672-678.

Augustine GJ and Charlton MP (1986) Calcium dependence of presynaptic calcium current and post-synaptic response at the squid giant synapse. *J Physiol (Lond)* **381:**619-640.

Burgess DL and Noebels JL (1999) Voltage-dependent calcium channel mutations in neurological disease. *Ann NYAcad Sci* **868:**199-212.

Campbell DB and Hess EJ (1999) L-type calcium channels contribute to the *tottering* mouse dystonic episode. *Mol Pharmacol* **55:**23-31.

Cruz LJ, Gray WR, Olivera BM, Zeikus RD, Kerr L, Yoshikami D and Moczydlowski E (1985) *Conus geographus* toxins that discriminate between neuronal and muscle sodium channels. *J Biol Chem* **260:**9280-9288.

Day NC, Wood SJ, Ince PG, Volsen SG, Smith W, Slater CR and Shaw PJ (1997) Differential localization of voltage-dependent calcium channel α_1 subunits at the human and rat neuromuscular junction. *J Neurosci* **17:**6226-6235.

De Luca A, Rand MJ, Reid JJ and Story DF (1991) Differential sensitivities of avian and mammalian neuromuscular junctions to inhibition of cholinergic transmission by ω-conotoxin GVIA. *Toxicon* **29:**311-320.

Etheredge JA, Murchison D, Abbott LC, Griffith WH (2005). Functional compensation by other voltage-gated Ca^{2+} channels in mouse basal forebrain neurons with $Ca_{V2.1}$ mutations. *Brain Res* 2005 Dec 16; [Epub ahead of print].

Fatt P and Katz B (1952) Spontaneous subthreshold activity at motor nerve endings. *J Physiol (Lond)* **117**:109-128.

Fletcher CF, Lutz CM, O'Sullivan TN, Shaughnessy JD, Hawkes R, Frankel WN, Copeland NG and Jenkins NA (1996) Absence epilepsy in tottering mutant mice is associated with calcium channel defects. *Cell* **87:**607-617.

Fletcher CF, Tottene A, Lennon VA, Wilson SM, Dubel SJ, Paylor R, Hosford DA, Tessarollo L, McEnery MW, Pietrobon D, Copeland NG, and Jenkins NA (2001) Dystonia and cerebellar atrophy in Cacnala null mice lacking P/Q calcium channel activity. *FASEB J* **15:**1288-1290.

Flink MT and Atchison WD (2002) Passive transfer of Lambert-Eaton syndrome to mice induces dihydropyridine sensitivity of neuromuscular transmission. *J Physiol (Lond)* **543:**567-576.

Flink MT and Atchison WD (2003) Iberiotoxin-induced block of Ca^{2+}-activated K^{+} channels induces dihydropyridine sensitivity of ACh release from mammalian motor nerve terminals. *J Pharmacol Exp Ther* **305:**646-652.

Gertler RA and Robbins N (1978) Differences in neuromuscular transmission in red and white muscles. *Brain Res* **142**:160-164.

Gray DB, Bruses JL and Pilar GR (1992) Developmental switch in the pharmacology of Ca^{2+} channels coupled to acetylcholine release. *Neuron* **8:**715-724.

Hong SJ and Chang CC (1989) Use of geographutoxin II (μ-conotoxin) for the study of neuromuscular transmission in mouse. *Br J Pharmacol* **97:**934-940.

Jun K, PiedrasRenteria ES, Smith SM, Wheeler DB, Lee SB, Lee TG, Chin H, Adams ME, Scheller RH, Tsien RW and Shin HS (1999) Ablation of P/Q-type Ca^{2+} channel currents, altered synaptic transmission, and progressive ataxia in mice lacking the α_{1A}-subunit. *Proc Natl Acad Sci U S A.* **21:**15245-15250.

Kaja S, Van de Ven RC, Ferrari MD, Frants RR, Van den Maagdenberg AM and Plomp JJ (2006) Compensatory contribution of $Ca_v2.3$ channels to acetylcholine release at the neuromuscular junction of *Tottering* mice. *J Neurophysiol* **95**:2698-2704.

Katz E, Ferro PA, Weisz G and Uchitel OD (1996) Calcium channels involved in synaptic transmission at the mature and regenerating mouse neuromuscular junction. *J Physiol (Lond)* **497:**687-697.

Kriebel ME and Stolper DR (1975) Non-Poisson distribution in time of small- and large-mode miniature end-plate potentials. *Am J Physiol* **229**:1321-1329.

Leenders AG, van den Maagdenberg AM, Lopes da Silva FH, Sheng ZH, Molenaar PC, and Ghijsen WE (2002) Neurontransmitter release from tottering mice nerve terminals with reduced expression of mutated P- and Q- type Ca^{2+} -channels. *Eur J Neurosci* **15:**13-18.

Llinás RR, Sugimori M and Cherksey B (1989) Voltage-dependent calcium conductances in mammalian neurons. The P channel. *Ann N Y Acad Sci* **560:**103-111.

McLachlan EM and Martin AR (1981) Non-linear summation of end-plate potentials in the frog and mouse. *J Physiol (Lond)* **311:**307-324

McDonough S, Boland L, Mintz I and Bean B (2002) Interactions among toxins that inhibit N-type and P-type calcium channels. *J Gen Physiol*, **119:**313-328.

Neelands TR, King APJ and MacDonald RL (2000) Functional expression of L-, N–, P/Q-, and R-type calcium channels in the human NT2-N cell line. *J Neurophysiol* **84:**2933-2944.

Pagani R, Song M, McEnery M, Qin N, Tsien RW, Toro L, Stefani E and Uchitel OD (2004) Differential expression of α_1 and β subunits of voltage dependent Ca^{2+} channel at the neuromuscular junction of normal and P/Q Ca^{2+} channel knockout mouse. *Neuroscience* **123**:75-85.

Pietrobon D (2002) Calcium channels and channelopathies of the central nervous system. *Mol Neurobiol* **25:**31-50.

Plomp JJ, Vergouwne MN, Van Den Maagdenberg AM, Ferrari MD, Frants RR and Molenaar PC (2000) Abnormal transmitter release at neuromuscular junctions of mice carrying the tottering α_{1A} Ca^{2+} channel mutation. *Brain* **123:**463-471.

Prakash YS, Miller SM, Huang M and Sieck GC (1996) Morphology of diaphragm neuromuscular junctions on different fibre types. *J Neurocytol* **25**:88-100.

Qian J and Noebels JL (2000) Presynaptic Ca^{2+} influx at a mouse central synapse with Ca^{2+} channel subunit mutations. *J Neurosci* **20:**163-170.

Randall A and Tsien RW (1995) Pharmacological dissection of multiple types of Ca^{2+} channel currents in rat cerebellar granule neurons. *J Neurosci* **15:**2995-3012.

Robitaille R, Adler EM, and Charlton MP (1990) Strategic location of calcium channels at transmitter release sites of frog neuromuscular synapses. *Neuron* **5:**773-779.

Rosato Siri MD and Uchitel OD (1999) Calcium channels coupled to neurotransmitter release at neonatal rat neuromuscular junctions. *J Physiol (Lond)* **514:**533-540.

Santafe MM, Sabate MM, Garcia N, Ortiz N, Lanuza MA, Tomas J (2005). Changes in the neuromuscular synapse induced by an antibody against gangliosides. *Ann Neurol* **57**:396-407.

Santafe MM, Urbano FJ, Lanuza MA and Uchitel OD (2000) Multiple types of calcium channels mediate transmitter release during functional recovery of botulinum toxin type A-poisoned mouse motor nerve terminals. *Neuroscience* **95:**227-234.

Smith DO, Conklin MW, Jensen PJ and Atchison WD (1995) Decreased calcium currents in motor nerve terminals of mice with Lambert-Eaton myasthenic syndrome. *J Physiol (Lond)* **15:**115-123.

Sugiura Y and Ko CP (1997) Novel modulatory effect of L-type calcium channels at newly formed neuromuscular junctions. *J Neurosci* **17:**1101-1111.

Sugiura Y, Woppmann A, Miljanich GP and Ko CP (1995) A novel ω-conopeptide for the presynaptic localization of calcium channels at the mammalian neuromuscular junction. *J Neurocytol* **24**:15-27.

Tsien RW, Ellinor PT and Horne WA (1991) Molecular diversity of voltage-dependent Ca^{2+} channels. *Trends Pharmacol Sci* **12:**349-354.

Uchitel OD, Protti DA, Sanchez V, Cherksey BD, Sugimori M and Llinás R (1992) P-type voltage dependent calcium channel mediates presynaptic calcium influx and transmitter release in mammalian synapses. *Proc Natl Acad Sci USA* **89:**3330-3333.

Urbano FJ, Depetris RS and Uchitel OD (2001) Coupling of L-type calcium channels to neurotransmitter release at mouse motor nerve terminals. *Pflügers Arch* **441:**824-831.

Urbano FJ, Piedras-Renteria ES, Jun K, Shin HS, Uchitel OD and Tsien RW (2003) Altered properties of quantal neurotransmitter release at endplates of mice lacking P/Q-type Ca^{2+} channels. *Proc Natl Acad Sci USA* **100:**3491-3496.

Varadi G, Strobeck M, Koch S, Caglioti L, Zucchi C and Palyi G (1999) Molecular elements of ion permeation and selectivity within calcium channels. *Crit Rev Biochem Mol Biol* **34:**181-214.

Vautrin J and Kriebel ME (1991) Characteristics of slow-miniature endplate currents show a subunit composition. *Neuroscience* **41**:71-88.

Wakamori M, Yamazaki K, Matsunodaira H, Teramoto T, Tanaka I, Niidome T, Sawada K, Nishizawa Y, Sekiguchi N, Mori E, Mori Y and Imoto K (1998) Single tottering mutations responsible for the neuropathic phenotype of the P-type calcium channel. *J Biol Chem* **273:**34857-34867.

Xu YF, Hewett SJ and Atchison WD (1998) Passive transfer of Lambert-Eaton myasthenic syndrome induces dihydropyridine sensitivity of I_{Ca} in mouse motor nerve terminals. *J Neurophysiol* **80:**1056-1069.

Zhang JF, Randall AD, Ellinor PT, Horne WA, Sather WA, Tanabe T, Schwarz TL and Tsien RW (1993) Distinctive pharmacology and kinetics of cloned neuronal Ca^{2+} channels and their possible counterparts in mammalian CNS neurons. *Neuropharmacology* **32:**1075-1088.

Zhou YD, Turner TJ and Dunlap K. (2003) Enhanced G protein-dependent modulation of excitatory synaptic transmission in the cerebellum of the Ca^{2+} channel-mutant mouse, tottering. *J Physiol (Lond)* **547:**497-507.

Footnotes

This work was supported by NIH grant R01 NS051833 to W.D.A., in part by an Osserman/Sosin/McClure Fellowship to N.E.P. from the Myasthenia Gravis Association, and by a grant from the Muscular Dystrophy Association of America. The Leica confocal microscope was provided by funding from the Life Sciences Corridor Program of the Michigan Economic Development Corporation. Preliminary results from this research were presented at The Society for Neuroscience Annual Meeting in 2003 and 2004 and published in Society for Neuroscience Abstracts Pardo NE and Atchison WD (2003) Program New Orleans, LA: Society for Neuroscience. Online. And Pardo NE and Atchison WD (2004). Program. San Diego, CA: Society for Neuroscience. Online.

Figure Legends

Figure 1. *(A)* Summary of comparative effects of specific Ca^{2+} channel blockers and agonist on ACh release at *C57BL/6J-tg* and *wt* neuromuscular junctions. Preparations were incubated with 100 nM ω-AgaTx IVA, 3 μM ω- CgTx GVIA, 10 μM nimodipine, or 1 μM BayK 4866 for 1 h. ***(B)* Effect of nimodipine and BayK 8644 on quantal content of *tg*/*tg* and *wt* mouse neuromuscular junctions.** Preparations were incubated for 1 h with 10 μM of the L-type Ca^{2+} channel blocker, nimodipine. Data for effects of BayK 8644 on *m* of *tg*/*tg* mouse hemidiaphragm preparations were collected before (control) and after 1h of incubation with 1 μM BayK 8644 (BayK) and then following further incubation with 1 μM BayK for 45 min in the presence of nimodipine (10 μM). In both panels quantal content (*m*) was determined for each preparation using the ratio of the average EPP amplitude to the average MEPP amplitude before and after addition of specific drug or toxin. EPPs were elicited at a frequency of 0.5 Hz. Each value represents the mean ± S.E.M. of 6 *wt* and 7 *tg* individual preparations. Values are expressed as the percentage of *m* after treatment with the specific Ca^{2+} channel agonist or antagonist to that of the pretreatment value. The asterisk (*) indicates a value significantly different from the control pretreatment value ($p < 0.05$). In Panel B, values are expressed as the percentage of *m* from preparations after the addition of nimopidine to that of the same preparation before nimodipine treatment.

Figure 2. Effect of ω-agatoxin IVA (ω-Aga-IVA) concentration on EPP amplitude from *tg/tg* and *wt* neuromuscular junction preparations. Preparations were incubated with 50, 100 or 300 nM ω-Aga-IVA for 1 h. A given preparation was only exposed to a single [ω-Aga IVA]. EPPs were elicited at a frequency of 0.5 Hz. Values are expressed as the percentage of EPP amplitude from the ω-Aga IVA- treated preparations to that of the pretreatment. Each value represents the mean ± S.E.M of 3 individual preparations. The asterisk (*) indicates a value significantly different from the control pretreatment value ($p < 0.05$), while the cross (†) indicates a significant difference between the two genotypes.

Figure 3. Effect of ω-agatoxin IVA (ω-Aga-IVA) and ω-conotoxin MVIIC (ω-CTx MVIIC) on *m* and EPP amplitude from *tg/tg* and *wt* neuromuscular junction preparations. *(A)* Preparations were incubated with 100 nM ω-Aga-IVA or 5 μM ω-CTx MVIIC for 1 h. EPPs were elicited at a frequency of 0.5 Hz. Values are expressed as the percentage of quantal content (*m*) from the ω-Aga IVA and ω-CTx MVIIC treated preparations to that of the pretreatment value. Each value represents the mean ± S.E.M of 5 individual preparations. The asterisk (*) indicates a value significantly different from the control pretreatment value ($p < 0.05$), while the cross (†) indicates a significant difference between the two genotypes. *(B-C)* EPPs were recorded from neuromuscular junction preparations isolated from homozygote *tottering (tg/tg)* mice, and wildtype (*wt*) mice with no pharmacological treatment (black control trace) or treated

by incubation for 1 h with 100 nM ω-Aga IVA (red trace). Each tracing represents the average of at least 10 EPPs at a stimulation frequency of 0.5 Hz recorded from a single representative preparation.

Figure 4. Effect of ω-Conotoxin GVIA (ω- CTx GVIA) and SNX 482 on *m* and EPP amplitude from *tg/tg* and *wt* neuromuscular junctions. *(A-D).* EPPs were recorded from neuromuscular preparations isolated from *tg/tg* mice (upper panel), and *wt* mice (lower panel) without any treatment (black control trace), or treated by incubation for 1 h with 1 μM SNX 482 (blue trace), 3 μM ω- CTx GVIA (orange trace) separately or both toxins simultaneously (magenta trace) for 45 min. Each tracing represents the average of at least 10 EPPs at a stimulation frequency of 0.5 Hz recorded from a single representative preparation. *(E).* Preparations were incubated with 3 μM ω-CTx GVIA and 1 μM SNX 482 separately for 1h, followed by incubation with the two antagonists together. EPPs were elicited at a frequency of 0.5 Hz. Values are expressed as the percentage of quantal content from the ω-CTx GVIA and SNX 482 (alone, gray bars and in combination, black bar) -treated preparations to that of the pretreatment value. Each value represents the mean ± S.E.M of 7 *tg* and 5 *wt* individual preparations. The asterisk (*) indicates a value significantly different from the control pre-treated preparation ($p < 0.05$) of the same genotype. The cross (†) indicates a value significantly different between the two genotypes.

Figure 5. Immunostaining of *wt* and *tg* neuromuscular junctions using an anti-syntaxin antibody and α-Bungarotoxin. *EDL* muscles from *wt* animals were stained with an antibody against two molecular markers of the cellular elements that configure the neuromuscular junction: the acetylcholine receptor (AChR) (red) in muscle cells and syntaxin in nerve terminals (blue). Juxtaposition (pink regions) shows the superimposition of AChR and syntaxin. The topological correspondence of syntaxin with the AChR is almost complete for both genotypes (*tg* and *wt*, right and left column respectively). Scale bar = 15 μm

.

Figure 6. Confocal images and 3D rendering of pixel density distribution of α_{1A} subunits at representative *wt* and *tg* motor nerve terminals. *TS* muscle from *wt* and *tg* animals were stained with α-bungarotoxin (red) and an antibody against the α_{1A} subunit of Ca^{2+} channels (green). Juxtaposition (yellow regions) shows the superimposition of AChR and α_{1A} subunits. Note that in *wt* preparations (left column), α_{1A} subunit staining exhibits a punctate distribution over the surface of the α-bungarotoxin labeled end-plate, with a high degree of juxtaposition. This pattern of distribution was not observed in the *tg* preparations (right column). Scale bar = 10.8 μm for the *wt* and 10.9 μm for *tg* images.

Figure 7. Confocal images and 3D rendering of pixel density distribution of α_{1B} and α_{1E} subunits at representative *wt* and *tg* motor nerve terminals. *TS* muscle from *tg* mice were stained with α-bungarotoxin (red) and an antibody against the α_{1B} (left column) or α_{1E} (right column) subunits of Ca^{2+} channels (green). Juxtaposition (yellow mark) shows the superimposition of AChR and α_{1B} or α_{1E} subunits. These confocal images and 3D rendering of pixel density distribution of α_{1B} and α_{1E} subunits show what appears to be an increase in the pattern of expression of α_{1B} and α_{1E} subunits labeling with a distribution along the vicinity of the end-plates and with some degree of juxtaposition with the α-bungarotoxin-label. Scale bar = 26 μm for the α_{1B} and 20.3μm for α_{1E} images.

Figure 8. Relative pixel count of fluorescence corresponding to α_1 subunits at *wt* and *tg* neuromuscular junctions.

Average fluorescence levels after staining *TS* muscle preparations with an antibody against the α_{1A}, α_{1B}, α_{1C}, or α_{1E} subunits of Ca^{2+} channels. For each preparation, 3-5 surface nerve terminals were selected by eye for quantitation of fluorescence intensity. The average of relative pixel count for each α_1 subunit in *tg* terminals was normalized to the average of pixel count in wt mice. Each value represents the mean ± S.E.M of 3 *tg* and *wt* individual preparations.

Figure 9. Percentage of juxtaposition of α_1 Ca^{2+} subunits with AChR at *wt* and *tg* neuromuscular junctions. Values are taken from the data for all neuromuscular junctions

sampled as depicted in Figure 8. Percentage of juxtaposition of α-bungarotoxin (red) and an antibody against the various α_1 subunits of Ca^{2+} channels (green) was calculated by dividing the surface or each picture taken into a perfect square of 5 by 5 squares for a total of 25 inner squares. Each inner square in which the green and the red dyes were juxtaposed was taken as 4% of juxtaposition. For each preparation, 3-5 surface nerve terminals were selected by eye for quantitation of juxtaposition. Each value represents the mean ± S.E.M of 3 *tg* and *wt* individual preparations. Where no histogram is shown, no measurable α_1 subunit staining juxtaposed with that of α-bungarotoxin

Table 1. Electrophysiological measurements at *tottering* neuromuscular junctions

	tg/tg	*wt*
n (muscle)	381	36
EPP amplitude (mV)[2]	18.6 ± 0.6[3]	19.2 ± 0.7
MEPP amplitude (mV)	1.2 ± 0.03	1.1 ± 0.05
Quantal content[4]	16.4 ± 0.5	19.8 ± 1.4
MEPP frequency (s^{-1})	1.4 ± 0.3	1.0 ± 0.6

[1]Measurements from *tg/tg* and *wt* neuromuscular junctions were made before any drug treatment.

[2]All EPPs were evoked at 0.5 HZ, and were corrected and adjusted to a standard membrane potential (-75mV) in order to correct for changes in driving force that alter the postjunctional membrane potential.

[3]Data represent the mean ± S.E.M. of individual preparations which were pooled prior to any drug or toxin treatment.

[4]Quantal content (*m*) is calculated using the ratio of the mean amplitude of the corrected EPPs and MEPPs.

JPET Fast Forward. Published on September 18, 2006 as DOI: 10.1124/jpet.106.108670
This article has not been copyedited and formatted. The final version may differ from this version.

Fig. 1

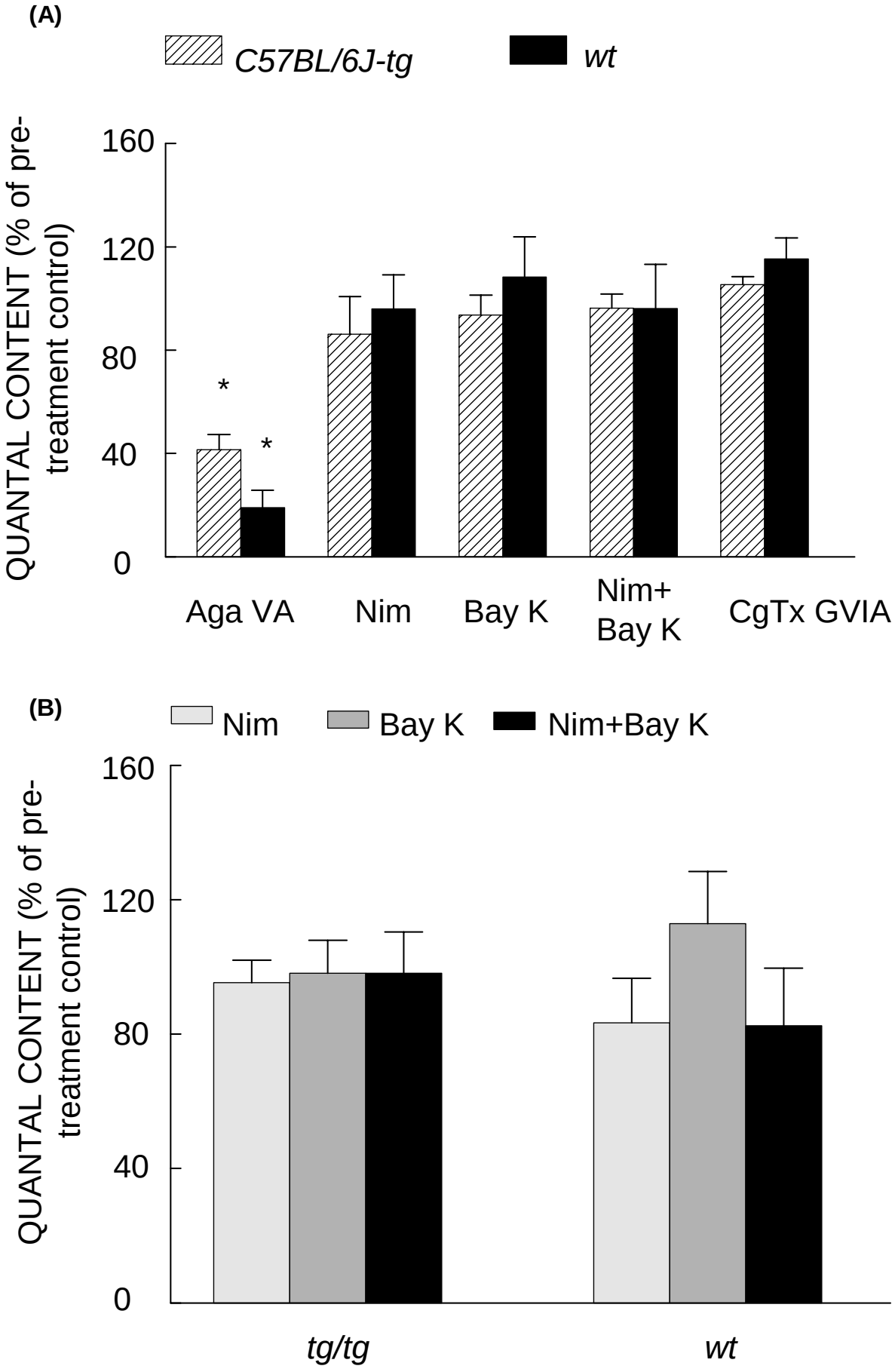

Fig. 2

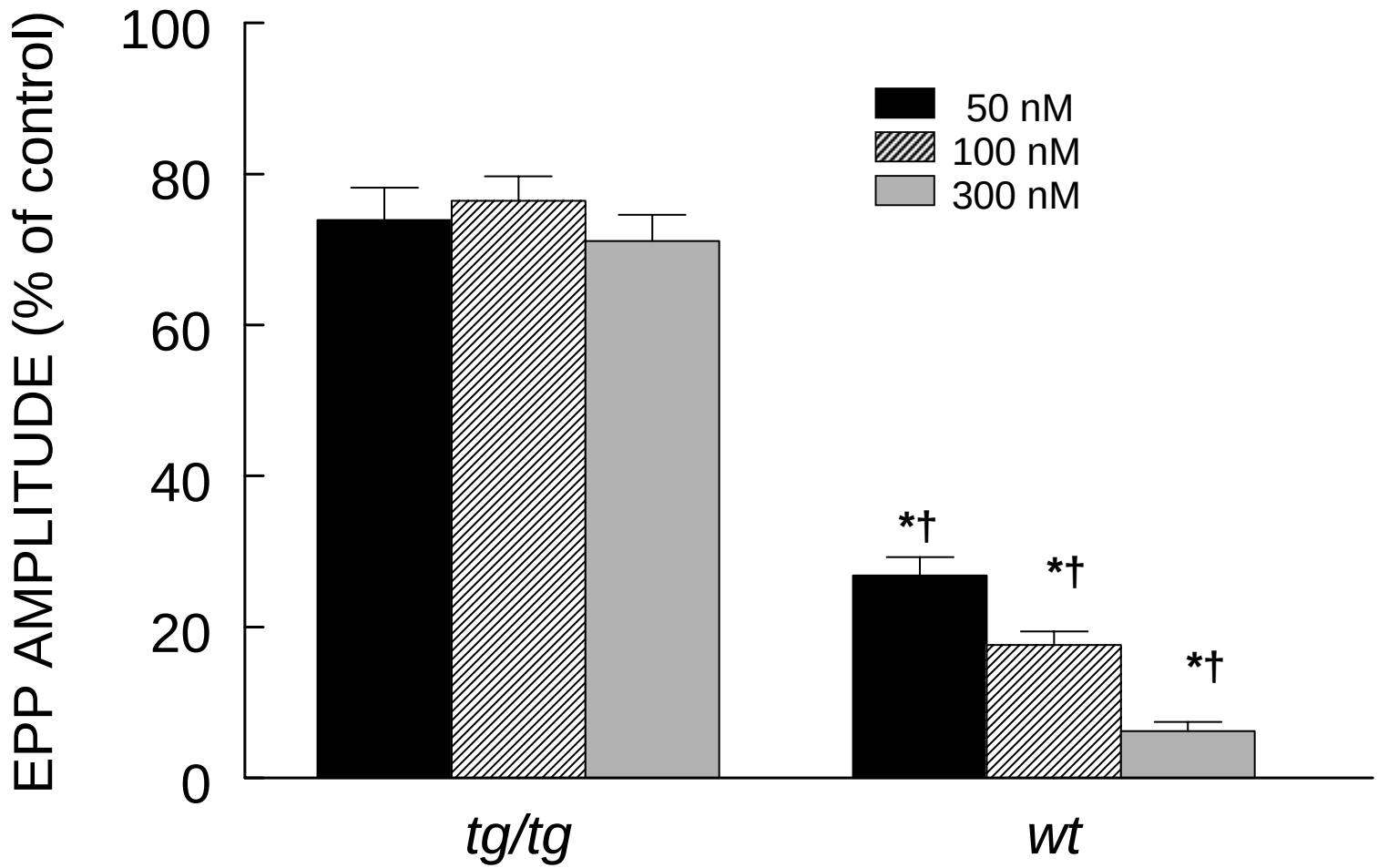

JPET Fast Forward. Published on September 18, 2006 as DOI: 10.1124/jpet.106.108670
This article has not been copyedited and formatted. The final version may differ from this version.

Fig. 3

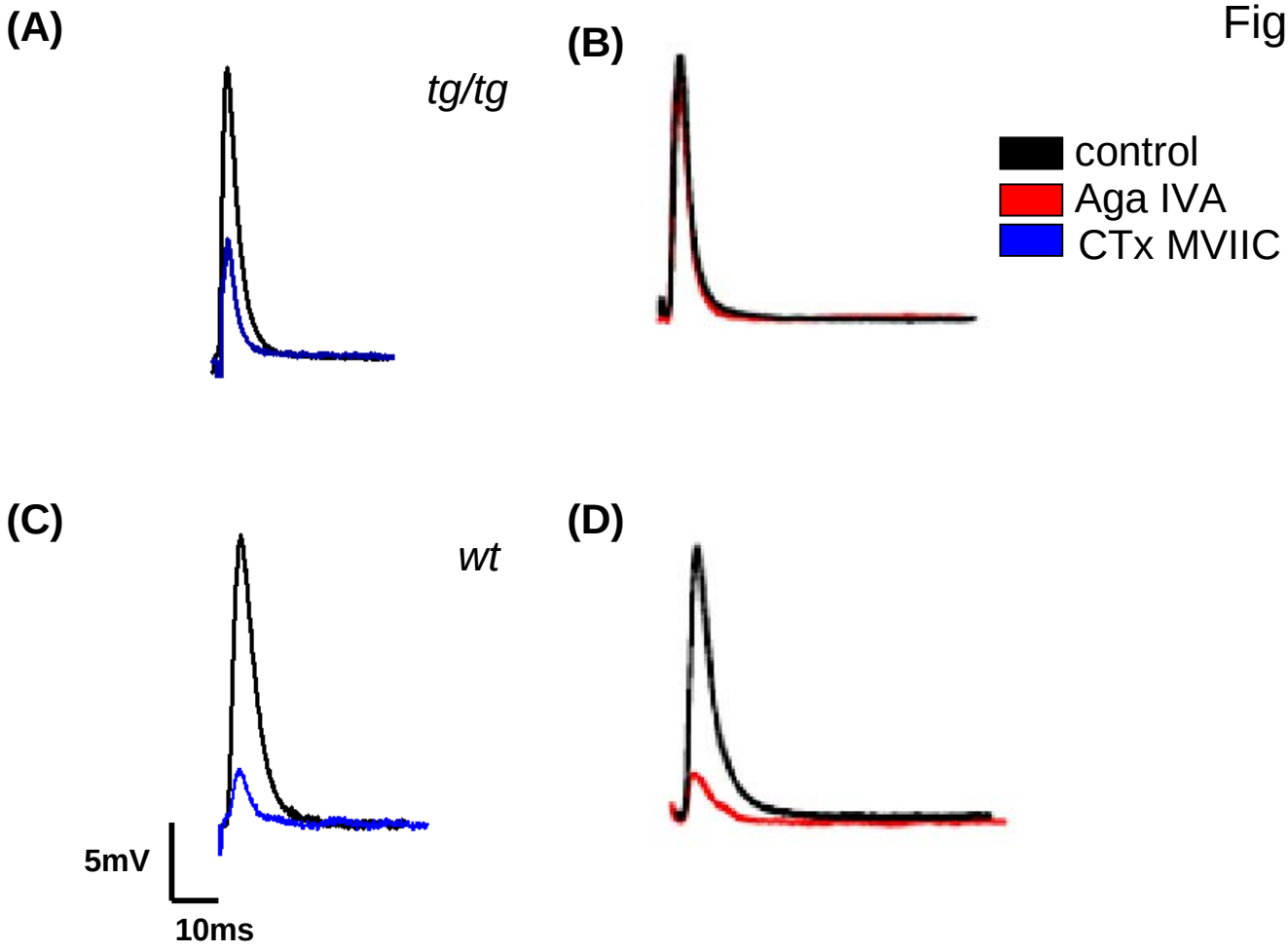

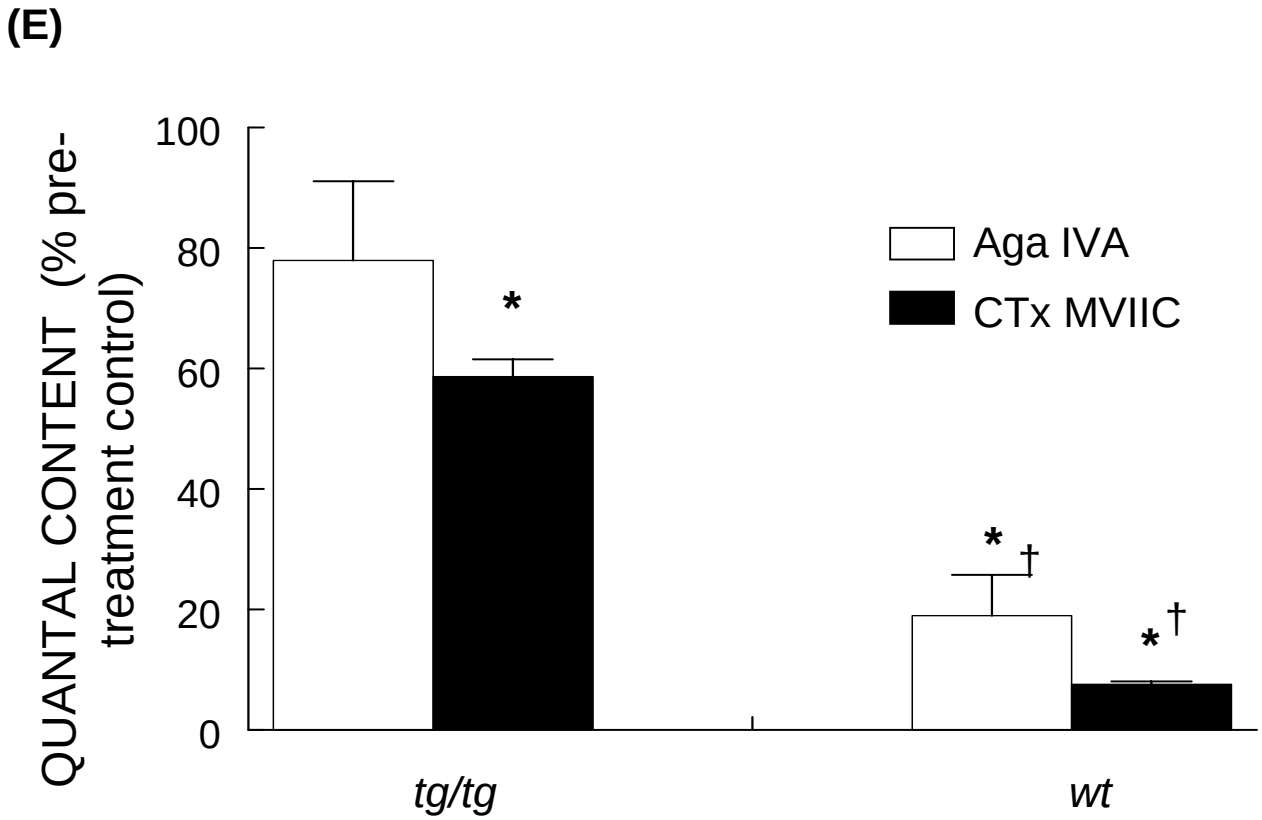

JPET Fast Forward. Published on September 18, 2006 as DOI: 10.1124/jpet.106.108670
This article has not been copyedited and formatted. The final version may differ from this version.

Fig. 4

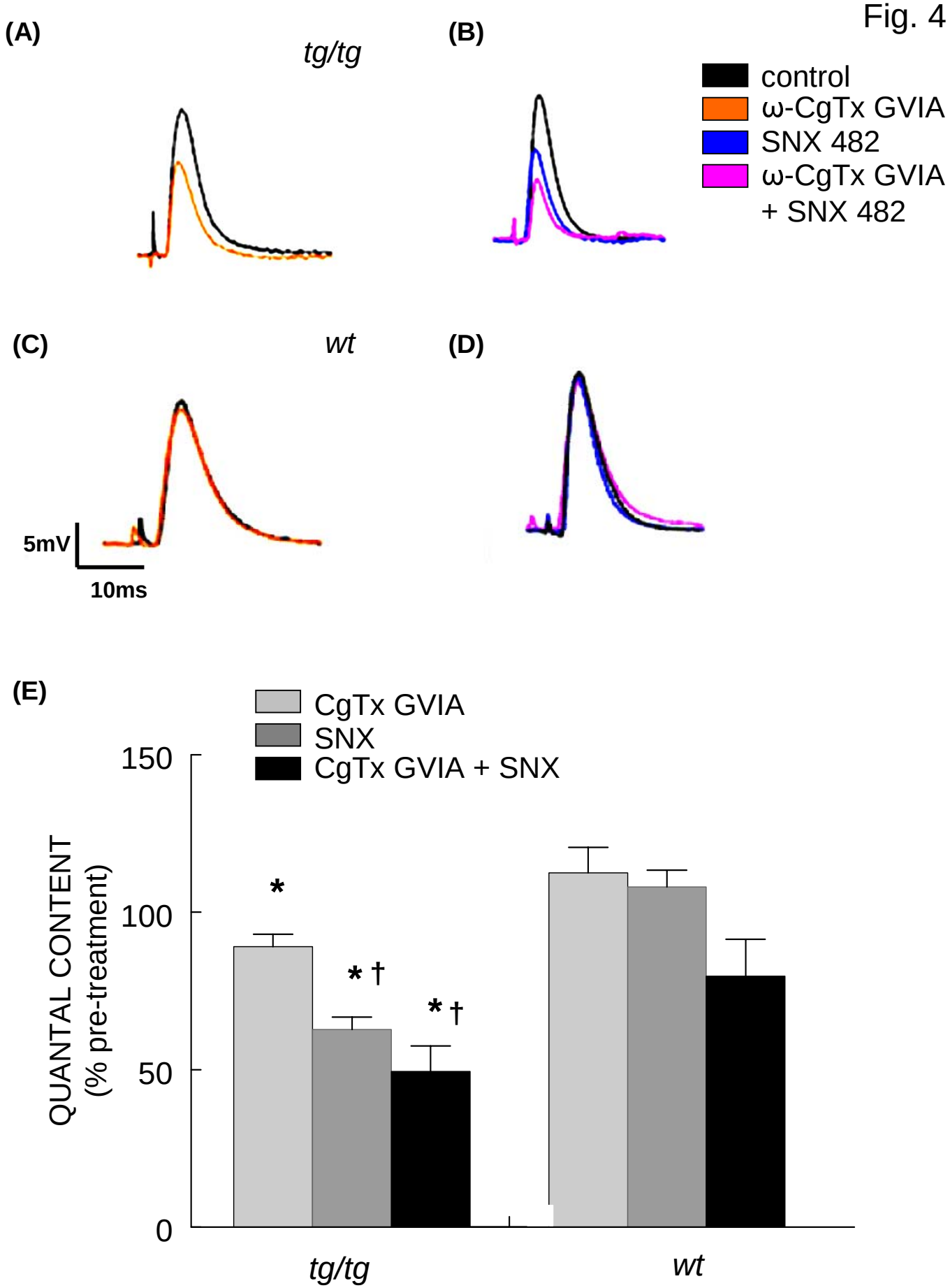

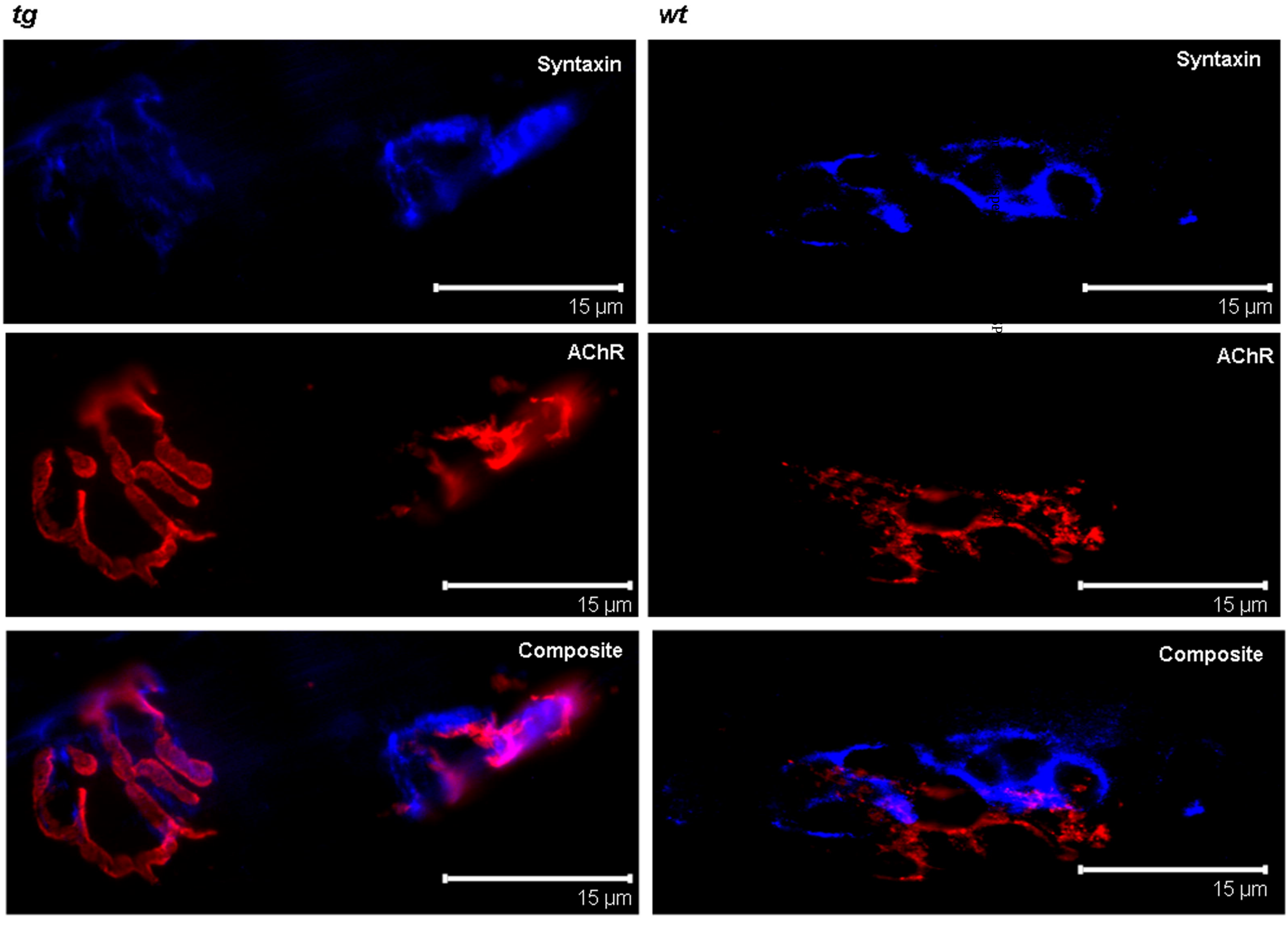
tg
wt
Syntaxin
15 µm
Syntaxin
15 µm
AChR
15 µm
AChR
15 µm
Composite
15 µm
Composite
15 µm

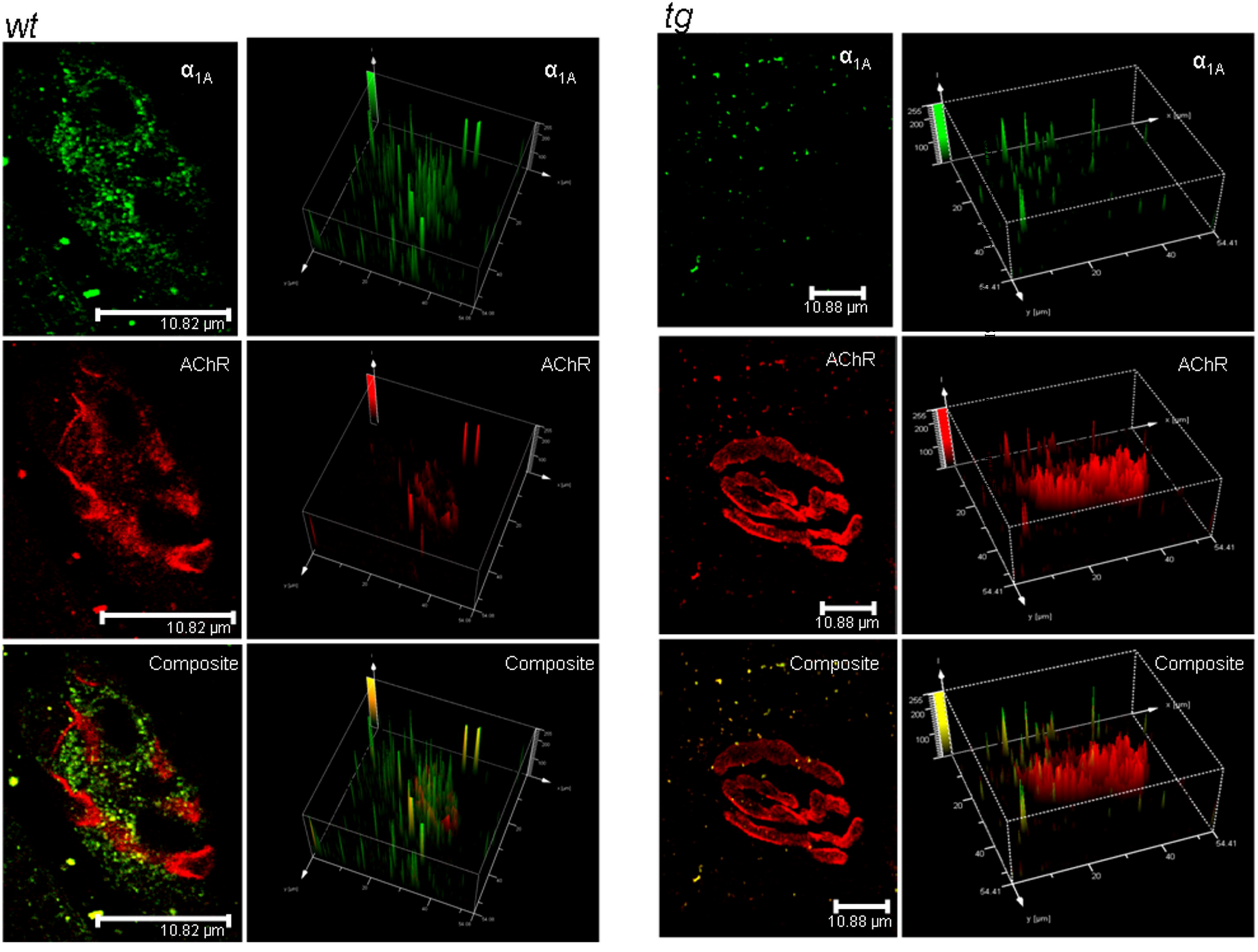
wt
tg
α1A
AChR
Composite
10.82 µm
10.88 µm

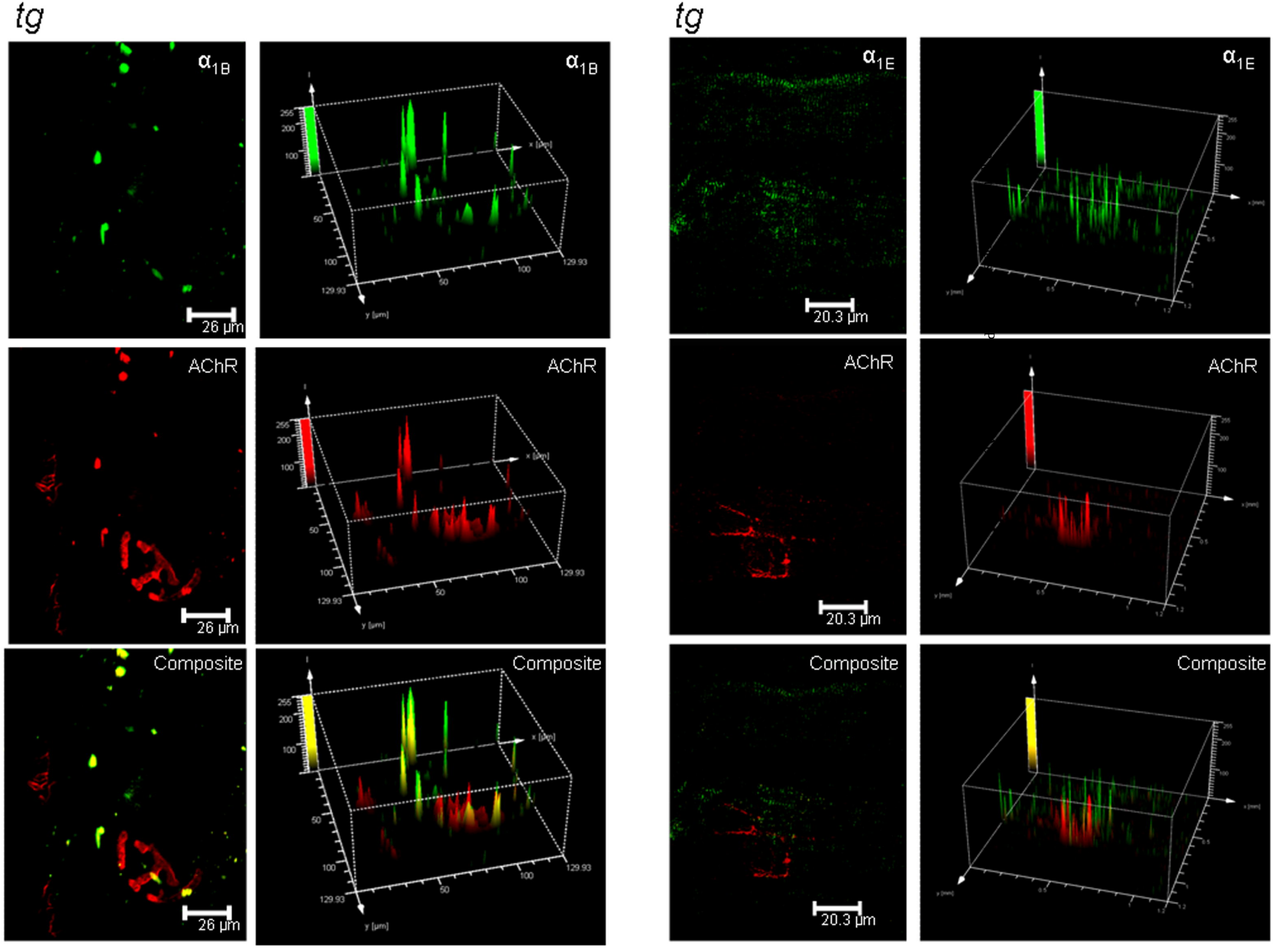
tg
α_{1B}
26 µm
α_{1B}
AChR
26 µm
AChR
Composite
26 µm
Composite
tg
α_{1E}
20.3 µm
α_{1E}
AChR
20.3 µm
AChR
Composite
20.3 µm
Composite

Fig. 8

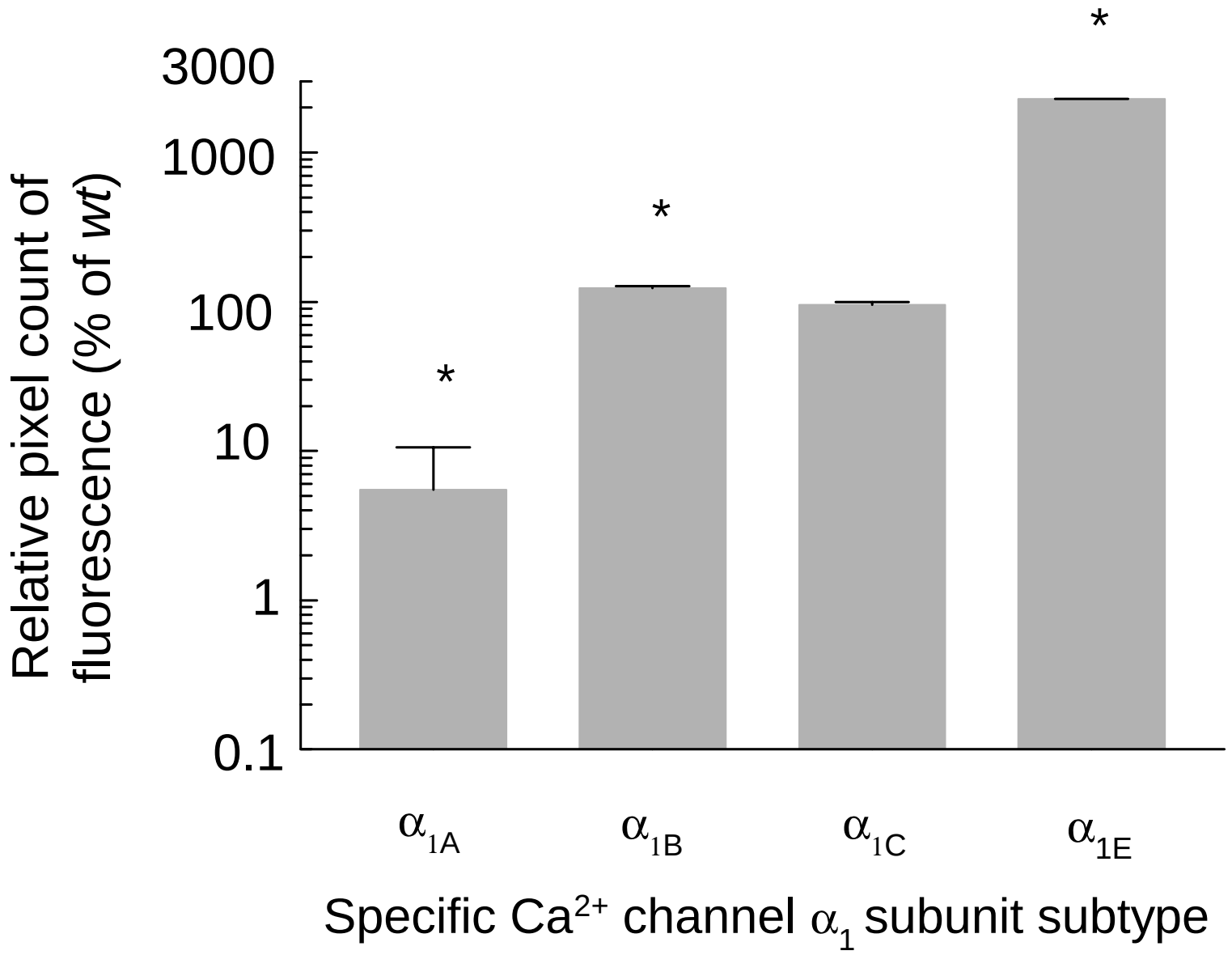

Fig. 9